Nanomaterials in Lateral Flow Assay

Arash Mohammadinejad, Ghazaleh Aleyaghoob, and Yavuz Nuri Ertas

Abstract Point-of-care devices have garnered the interest of scientists in recent years due to their capacity for on-site, bedside, and in-home surveillance in many fields of the medical, biological, pharmaceutical, and food sciences and industries. These devices can be categorized primarily as either portable or stationary. Due to their simple downsizing, mobility, low cost, and low power consumption, portable devices have attracted a great deal of interest. Recently, lateral flow assays have gained popularity as a portable platform due to the simplicity of strip design and the ability to detect with the naked eye. As inseparable components of lateral flow assay, nanomaterials have played a prominent role in enhancing sensitivity due to their large surface area, ease of functionalization, and tunable physical and chemical characteristics based on size, shape, and composition. The conventional lateral flow approach is an immunoassay in which gold nanoparticles with a unique plasmonic surface property show a red color on the test and control lines to enable qualified detection. This approach, with its quantitative limitations and limited sensitivity, is essential for the introduction of novel nanoparticles. Numerous nanoparticles, including quantum dots, carbon nanotubes, magnetic nanoparticles, nanoenzymes, surface-enhanced Raman scattering nanotags, upconversion nanoparticles, and time-resolved fluorescence nanoparticles, have been utilized in the design of lateral flow assays to date. This chapter focuses mostly on the characteristics of various nanoparticles combined with lateral flow assay and associated transduction method for readout of signals produced by nanoparticles, as well as a critical analysis of the resulting approaches.

A. Mohammadinejad · Y. N. Ertas (✉)
ERNAM—Nanotechnology Research and Application Center, Erciyes University, Kayseri 38039, Türkiye
e-mail: yavuznuri@gmail.com

A. Mohammadinejad · G. Aleyaghoob
Department of Medical Biotechnology and Nanotechnology, School of Medicine, Mashhad University of Medical Sciences, Mashhad, Iran

Y. N. Ertas
Department of Biomedical Engineering, Erciyes University, Kayseri 38039, Türkiye

A. K. Mandal et al. (eds.), *Functionalized Smart Nanomaterials for Point-of-Care Testing*, Smart Nanomaterials Technology,
https://doi.org/10.1007/978-981-99-5787-3_3

Keywords Point-of-care · Lateral flow assay · Nanomaterial · Biosensor · Immunoassay

1 Introduction

Point-of-care (POC) devices have attracted unprecedented attention in recent years due to their exceptional significance in the self-testing of biological, food, and pharmaceutical samples, among others, with the benefits of high speed, low cost, sensitivity, on-site, and user-friendly detection. The majority of the success of point-of-care (POC) devices may be attributed to the limitations of established procedures such as liquid chromatography coupled with tandem mass spectrometry (LC-MS/MS), real-time polymerase chain reaction (qPCR), and enzyme-linked immunosorbent assay (ELISA) [1]. These approaches mostly suffer from the disadvantages of a lengthy procedure, a necessity for a high level of skill, and costly equipment, which might limit their use [2]. Therefore, scientists have a significant interest in the development and introduction of rapid reactions, simple procedures, inexpensive and individual-centered detection technologies.

Lateral flow assay (LFA), a paper-based approach, may significantly assist the objectives of POC technology for the advancement of home testing. This method enables the qualitative and quantitative detection of a wide range of targets, including proteins, antibodies, nucleic acids, whole cells, toxicants, drugs, etc., on a simple, low-cost platform with a negligible sample volume [3]. The standard structure of the LFA strip (4–6 mm × 6–7 cm) includes a sample pad, conjugate pad, detection pad (nitrocellulose membrane), adsorbent pad, and backing pad. These components are composed of cellulose, glass fiber, nitrocellulose membrane, cellulose, and polystyrene**,** respectively [4]. Following the assembly of the sample pad, conjugate pad, detection pad, and adsorbent pad on the backing pad, an appropriate amount of reporter particle-conjugated bioreceptor (antibody, aptamer, or DNA) can be deposited on the conjugated pad for the subsequent operation. The loading of sample onto the sample pad results in the formation of a complex between the target and reporter particle-conjugated bioreceptor, followed by the target's movement toward the adsorbent pad. During the passage of nitrocellulose membrane, the target complex interacts with the detection zone on the membrane including the test line (T-line) and control line (C-line) formed by dispensing bioreceptor of the target (antibody, aptamer, and DNA) and anti-immunoglubin (or complementary nucleic acid strand) on the nitrocellulose membrane, respectively [1]. Depending on the nature of the reporter particle, in the presence and absence of the target, characteristic lines can appear on the T-line or C-line that can be recognized with the naked eye or an instrument.

Despite the numerous advantages of LFA, its application may be limited by several drawbacks. Possibility of nonspecific interactions with the sample matrix in the nitrocellulose pores and saturation of detection zones (T-line and C-line) at high concentrations of analyte, leading to false responses, are downsides of LFA. The

solution to these issues is sample dilution, which may result in decreased sensitivity. Thus, there has been a need for signal amplification, which may be accomplished by combining nanotechnology with LFA technology [5].

Nanomaterials with high surface area, stability, conductivity, and simple functionalization can enhance the detection systems' sensitivity, specificity, reproducibility, repeatability, accuracy, and dependability [6]. The expanding use of nanomaterials in biosensor production has led to the development of portable, miniaturized transduction platforms [7]. Biosensors based on nanomaterials offer ultrasensitive, fast, and concurrent multiple detection of targets, early stage disease diagnosis and on-time therapy, and little sample consumption [8–10]. The development of nanotechnology can facilitate the construction of POC devices, such as LFA or microfluidic devices, that offer tailored molecular detection in several domains, such as food safety monitoring, diagnostic medicine, etc. Due to the significant dependence of LFA development on nanotechnology, this chapter focuses on the nanomaterials used in the design of LFAs. In addition to describing characteristics and critical topics, detection methods and transduction systems are classified based on the nanomaterials' application.

2 Nanomaterials

In recent years, nanomaterials, particularly metallic nanoparticles (NPs), have been widely used in the design of biosensors and POC devices due to their impressive properties, which include a higher surface area to volume ratio ($>10^7$:1) with small size (1–100 nm) compared to macro-sized particles, and inimitable chemical, physical, optical, magnetic, and electrical properties that enable the integration of different transducers with the LFA method [11, 12]. Due to the enhancement of LFA's potential for both quantification and qualification purposes, it has become necessary to use nanoparticles as labels with LFA. In addition to increasing the required sensitivity for quantification detections, this technology can provide signals that can be read by a variety of transducer systems. As depicted in Fig. 1, numerous nanoparticles have been utilized in the implementation of LFA platforms, including gold nanoparticles (AuNPs), which are widely used as label nanoparticles in colorimetry, quantum dots (QDs), carbon nanotubes (CNTs), magnetic nanoparticles (MNPs), nanoenzymes, surface-enhanced Raman scattering (SERS)-nanotags, upconversion nanoparticles (UCNPs), etc. [4, 13]. Table 1 offers an overview of the different nanoparticles and related transduction processes used for LFA signal reading.

2.1 AuNPs

AuNPs have several benefits that increase their applicability in a broad range of disciplines, including healthcare, engineering, the sciences, etc. Scientists are interested

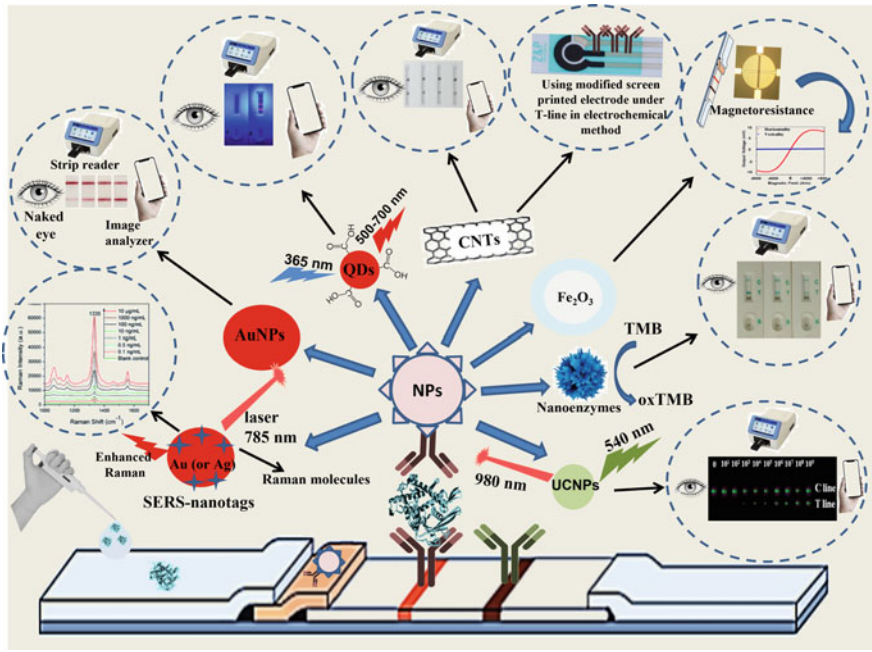

Fig. 1 Application nanoparticles in LFA and possible transduction systems

in the possibility of AuNPs being used in the design of biosensors for diagnosis and therapy, among other uses. These advantages include high safety, redox capability, catalytic behavior, substantial biocompatibility, great conductivity, a high surface-to-volume ratio, surface plasmon resonance (SPR), simple detection of its red color with the naked eye, and simple bioconjugation by antibodies, oligonucleotides, and proteins [51]. Due to the aforementioned characteristics, AuNPs have been predominantly utilized as colorimetric markers for LFAs. In addition, additional approaches, such as electrochemical, SPR, etc., can be combined with LFAs due to the physical and chemical characteristics of AuNPs.

Optical biosensors capable of visual detection of targets with an inexpensive and simple transducer that generates a signal proportional to the concentration of the target. This signal can represent quantifiable changes in the properties of light, such as its intensity, refraction index, and resonance frequency. Nanomaterials can generate light or its variations by transferring electrons between energy levels, resulting in diverse ways such as fluorescence, absorption, colorimetric, luminescence, refractometry, and SPR [52]. Due to the great sensitivity and ease of transduction of signals, which can be conducted with the naked eye, optical detection of LFA signals has been the most often used method in the literature [53]. Due to the straightforward appearance of color on the T-line or C-line, the colorimetric readout has garnered a great deal of attention for inclusion with LFAs, resulting in greater compatibility with the goals of POC devices. Due to the special characteristics of SPR, the application of AuNPs in LFAs has been extensively documented.

Table 1 Summarized data of studies designed LFA based on various NPs

NPs	Target	Detection process	Transduction
AuNPs	Troponin I	Binding of AuNP (40 nm) to AuNP (10 nm)-antibody	Colorimetric
AuNPs	C-reactive protein (CRP)	Automatic sensitivity enhancement using $KAuCl_4$ and $NH_2OH \cdot HCl$ in the presence of AuNP-antibody	Colorimetric
AuNPs	Human immunodeficiency virus type 1 (HIV-1) target nucleic acid	Aggregation of oligonucleotide-conjugated AuNPs on the AuNP-antibody	Colorimetric
AuNPs	Embryonic antigen (CEA) as tumor biomarker Procalcitonin, (PCT) as bacterial infection biomarker	Catalytic activity of horseradish peroxidase (HRP) on the AuNP-antibody for luminol and H_2O_2	Colorimetric (GLFT) & chemiluminescence (C-mode GLFT)
AuNPs	Ochratoxin A	Deposition of silver on the AuNP-antibody using hydroquinone	Colorimetric
AuNPs	Zearalenone (ZEN)	Oxidative polymerization of dopamine on the AuNPs	Colorimetric
AuNPs	Dengue NS1 Protein	Conjugation of ferrocene-antibody on AuNPs-labeled antibody	Electrochemical

(continued)

Table 1 (continued)

NPs	Target	Detection process	Transduction
AuNPs	8-hydroxy-2′-deoxyguanosine (8-OHdG)	1-Evaluation of color of AuNPs-antibody on the T-line (8-OHdG-antibody/antigen) 2-Evaluation of current reduction by capturing free AuNPs-antibody or AuNPs-antibody/8-OHdG on C-line (8-OHdG-antibody)	Colorimetric & electrochemical
AuNPs	Hepatitis B virus (HBV) DNA	Automatic assay by migration of Au^{3+} and binding DNA hybridization on T-line resulted in AuNPs formation	Electrochemical
AuNPs	C-reactive protein (CRP)	Oxidation of $Ru(bpy)_3^{2+}$-labeled AuNPs and tripropylamine (TPA)	Electrochemiluminescent
CNTs	Methamphetamine (MET)	MWCNTs-labeled antibody/antigen on the T-line	Colorimetric
CNTs	Squamous cell carcinoma antigen (SCCA)	Cotton thread immunochromatographic using CNTs@ AuNPs-antibody	Colorimetric
Amorphous carbon nanoparticles (ACNPs)	*Fusarium* mycotoxins (Zearalenone, T-2 Toxin, Deoxynivale)	ACNPs-labeled antibody/antigen captured on T-line	Colorimetric
Carbon dots (CDs)	Zearalenone (ZEN)	Quenching the CD-ovalbumin by AgNPs-antibody	Fluorimetric

(continued)

Table 1 (continued)

NPs	Target	Detection process	Transduction
CNTs	Chlorpyrifos oxon (CPO)	Difference between activation of acetylcholinesterase (AChE) and CPO-AChE on CNT-modified Screen-Printed Electrode (SPE) T-line on	Electrochemical
Graphite-like carbon nitride (g-C3N4)	17β-estradiol (E2)	g-C_3N_4@AuNPs—antibody/antigen on the T-line	Colorimetric
CdTe quantum dots (QDs)	HIV-DNA	Displacement amplification technology between hairpin H1-strand, H2-CdTe QDs, and HIV-DNA	Fluorimetric
Core/shell CdSe/ZnS QDs	Fumonisin mycotoxins	Quenching the QDs@antigen by AgNPs or AuNPs-labeled antibody	Fluorimetric
ZnSe/CdSe core capped with CdS/$Cd_xZn_{1-x}S$/ZnS multishell	Human hepatitis B surface Antigen	QD-labeled antibody/antigen captured on the T-line	Fluorimetric
$CuInZn_xS_{2+x}$ ($x = 1$) capped by ZnS// ZnS	CRP	QD-labeled antibody/antigen captured on the T-line	Fluorimetric
Silica particles porous loaded CdSe/ CdS/ZnS QDs	CRP	QD-labeled antibody/antigen captured on the T-line	Fluorimetric
Quantum dot nanobead (QB)	Aflatoxin B_1 (AFB_1) and zearalenone (ZEN)	QB-labeled antibody/antigen captured on the T-line	Fluorimetric
Fe_2O_3–AuNPs Magnetic nanoparticles (MnGMs)	Aflatoxin B2 (AFB2)	MnGMs-labeled antibody/antigen captured on the C-line	Colorimetric
Fe_2O_3–SiO_2	Hepatitis B surface antigen (HBsAg)	Fe_2O_3@SiO_2-labeled antibody/ antigen captured on the T-line	Magnetometric

(continued)

Table 1 (continued)

NPs	Target	Detection process	Transduction
Streptavidin-modified magnetic nanoparticles (MNP-SA)	*L. monocytogenes* cells	Magnetically enrichment of *L. monocytogenes* through streptavidin and biotin interaction followed by extraction of DNA and detection by AuNP-probe	Colorimetric
Magnetic beads-protein G	Troponin I (cTnI)	Magnetic beads@protein G@antibody/antigen captured on the T-line	Magnetometric
Magnetic beads-COOH	Neuron-specific enolase (NSE) and carcinoembryonic antigen (CEA)	Magnetic beads- antibody/antigen captured on the T-line	Magnetometric
AuNPs@ platinum	Human prostate-specific antigen (PSA)	AuNPs@platinum-antibody/antigen captured on the T-line followed by addition TMB/H_2O_2	Colorimetric
AuNPs@ platinum nanowire	Rabbit IgG	AuNPs@ platinum-antibody/antigen captured on the T-line followed by addition of 3-amino-9-ethyl-carbazole (AEC)/ H_2O_2	Colorimetric
AuNPs@ platinum nanowire	p24 (biomarker of HIV)	AuNPs@ platinum@antibody/ antigen captured on the T-line followed by addition 4-Chloro-1-naphthol/ 3,3′-Diaminobenzidine, tetrahydrochloride (CN/DAB) /H_2O_2	Colorimetric

(continued)

Table 1 (continued)

NPs	Target	Detection process	Transduction
Palladium-platinum (Pd–Pt) nanoparticles	*Escherichia coli* O157:H7	Pd–Pt-labeled anibody/antigen captured on the T-line followed by addition TMB/H_2O_2	Colorimetric
$NaYF_4$:Yb, Tm@ $NaYF_4$ @Ca^{2+} upconversion nanoparticles (UPC	*Avian influenza virus (AIV)*	$NaYF_4$:Yb, Tm@ $NaYF_4$ @Ca^{2+}-labeled antibody/antigen captured on the T-line	Fluorimetric
Europium-chelate	Phospholipase A2 receptor (anti-PLA2R-IgG)	Europium-chelate-antibody/antigen captured on the capture antibody on the surface of well	Fluorimetric
Reporter-labeled hollow gold nanospheres (HGNs)	Staphylococcal enterotoxin B (SEB)	HGNs-labeled antibody/antigen captured on the T-line	SERS
Flower-like gold-silver core-shell bimetallic nanoparticles (AuNF@Ag)	β-adrenergic agonist brombuterol (BB)	AuNF@Ag-labeled antibody/antigen captured on the C-line	SERS
Au@Ag NPs @ two layers of Raman dye 5,5′-dithiobis-(2-nitrobenzoic acid) (Au@DTNB@Ag@DTNB)	Human IgM	Au@DTNB@Ag@DTNB-antibody/antigen captured on the T-line	SERS
Au nanorod (AuNR)@Raman tags@Au	cTnI	Au nanorod (AuNR)@Raman tags@Au-antibody/antigen captured on the T-line	SERS

(continued)

Table 1 (continued)

NPs	Linear range	LOD	Real sample	Time (min)	References
AuNPs	0.10–14.27 ng/mL	0.01 ng/mL	Serum samples of patients with myocardial infarction	10	[14]
AuNPs	0.1 − 5 μg/mL	0.001 μg/mL	Human serum samples	15	[15]
AuNPs	0.1–25 nM	0.1 nM	N.M	20	[16]
AuNPs	GLFT:CEA 10–200 ng/mL PCT 10–10^3 pg/mL C-mode GLFT:CEA 5–200 ng/mL PCT 10–10^4 pg/mL	GLFT:CEA 0.17 ng/mL PCT 10 pg/mL C-mode GLFT:CEA 0.0017 ng/mL PCT 0.05 pg/mL	Whole blood	GLFT: 15 C-mode GLFT:30	[17]
AuNPs	1–20 μg/L	0.9 μg/L	Wines and grape must samples	20	[18]
AuNPs	0.01–50 ng/mL	7.4 pg/mL	Maize	30	[19]
AuNPs	1–25 ng/mL	0.5 ng/mL	N.M	15	[20]
AuNPs	1–200 ng/mL	Colorimetric: 5.76 ng/mL Electrochemical: 8.85 ng/mL	Urine	10	[21]
AuNPs	10 pM–2 μM	7.23 pM	Human serum sample	7	[22]
AuNPs	0.01 − 1000 ng/mL	4.6 pg/mL	Serum	15	[23]
CNTs	62.5–1500 ng/mL	N.M	Human serum, urine, and saliva	30	[24]
CNTs	5–500 ng/mL	3.03 ng/mL	Human serum	20	[25]

(continued)

Table 1 (continued)

NPs	Linear range	LOD	Real sample	Time (min)	References
Amorphous carbon nanoparticles (ACNPs)	Deoxynivalenol 18.75–600 μg/kg T-2 Toxin 9.375–300 μg/kg Zearalenone 0.938–30 μg/kg	Deoxynivalenol 20 μg/kg T-2 Toxin 13 μg/kg Zearalenone 1 μg/kg	Maize	8	[26]
Carbon dots (CDs)	N.M	1–2.5 μg/kg	Cereal samples and their products	5	[27]
CNTs	1.0−200 nM	N.M	Human red blood cells (RBCs) sample	2	[28]
Graphite-like carbon nitride (g-C3N4)	0.25–10 ng/mL	0.5 ng/mL	Food samples including fish, prawn, pork, and chicken	10	[29]
CdTe quantum dots (QDs)	1 pM–10 nM	0.76 pM	Human serum	15	[30]
Core/shell CdSe/ZnS QDs	N.M	62.5 μg/kg	Maize flour samples	15	[31]
ZnSe/CdSe core capped with CdS/$Cd_xZn_{1-x}S$/ZnS multishell	N.M	0.05 ng/mL	N.M	20	[32]
$CuInZn_xS_{2+x}$ ($x = 1$) capped by ZnS//ZnS	0–800 ng/mL	5.8 ng/mL	N.M	3	[33]
Silica particles porous loaded CdSe/CdS/ZnS QDs	0–6.25 ng/mL	0.036 mg/L	Blood samples	15	[34]
Quantum dot nanobead (QB)	2–300 pg/mL	AFB_1 1.65 pg/ mL ZEN 59.15 pg/ mL	Maize extracts	15	[35]

(continued)

Table 1 (continued)

NPs	Linear range	LOD	Real sample	Time (min)	References
Fe_2O_3–AuNPs Magnetic nanoparticles (MnGMs)	N.M	0.9 ng/ml	Peanut, hazelnut, pistacia, and almond	15	[36]
Fe_2O_3–SiO_2	N.M	0.1 pg/mL	Clinical sera specimens	N.M	[37]
Streptavidin-modified magnetic nanoparticles (MNP-SA)	N.M	3.5×10^4 CFU/g	Lettuce samples	1	[38]
Magnetic beads-protein G	0.01–12.5 ng/mL	0.01 ng/mL	N.M	N.M	[39]
Magnetic beads-COOH	0–100 ng/mL	NSE ng/mL 0.094 CEA 0.045 ng/mL	Serum sample	30	[40]
AuNPs@ platinum	10–200 pg/mL	3.1 pg/mL	Plasma	5	[41]
AuNPs@ platinum nanowire	0.05–10 ng/mL	5 pg/mL	Plasma	5	[42]
AuNPs@ platinum nanowire	0.2–10 ng/mL	0.8 pg/mL	Plasma	20	[43]
Palladium-platinum (Pd–Pt) nanoparticles	$1 \times 10^3 - 1 \times 10^6$ cfu/mL	1×10^3 cfu/mL	Milk	25	[44]
$NaYF_4$:Yb, Tm@ $NaYF_4$ @Ca^{2+} upconversion nanoparticles (UPC)	LPAI H5N2 $10^{0.5}$ to 10^4 EID_{50} (50% egg infective dose)/mL HPAI H5N6 $10^{2.5}$–10^5 EID_{50}/mL	LPAI H5N2 10^2 EID_{50}/mL HPAI H5N6 $10^{3.5}$ EID_{50}/mL	Oropharyngeal and cloacal swabs	20	[45]
Europium-chelate	0.03–340 mg/L	0.03 mg/L	Human serum	5	[46]

(continued)

Table 1 (continued)

NPs	Linear range	LOD	Real sample	Time (min)	References
Reporter-labeled hollow gold nanospheres (HGNs)	0.1 pg/mL–1,000 ng/mL	0.001 ng/mL	N.M	6	[47]
Flower-like gold-silver core-shell bimetallic nanoparticles (AuNF@Ag)	N.M	0.5 pg/mL	Swine meat and urine samples	15	[48]
Au@Ag NPs @ two layers of Raman dye 5,5′-dithiobis-(2-nitrobenzoic acid) (Au@DTNB@Ag@DTNB)	0.1 ng/mL–10 μg/mL	0.1 ng/mL	*Mycoplasma pneumoniae* (MP)-specific IgM serum	N.M	[49]
Au nanorod (AuNR)@Raman tags@Au	0.1–100 ng/mL	0.1 ng/mL	Serum	10	[50]

N.M.: Not mentioned

In a straightforward and basic design of LFAs, antibody-conjugated AuNPs were utilized as the detection agent, resulting in sandwich immunocomplex formation and naked-eye detection by capturing antibody-immobilized sites on the nitrocellulose membrane [54]. In addition, colorimetric signals may be measured by using a strip analyzer or intensity image analyzer software. In this simple LFA design, the sensitivity may be enhanced by optimizing the size distribution of the AuNPs. A number of studies have revealed that the diameter of AuNPs significantly affects the sensitivity of AuNPs-based lateral flow immunoassays (LFIA) [14, 55]. In an enhanced design of LFA strips, two conjugation pads containing two distinct sizes of antibody-conjugated AuNPs have been implanted in order to increase sensitivity. The larger AuNPs can be attached to bovine serum albumin (BSA)-antibody, whereas the smaller antibody-conjugated AuNPs are inhibited by BSA [14]. The formation of a complex via BSA-antibody interaction on the T-line leads to the improvement of color and sensitivity by AuNPs with a greater size. Nylated ssDNA can also be used as a connection between AuNPs-streptavidin and AuNPs-labeled antibodies on the T-line or C-line [56]. The in situ increase of AuNPs size (Au deposition) on the T-line or C-line is an additional technique for sensitivity amplification. In the presence of hydroxylamine hydrochloride, the catalytic effect of AuNPs on the reduction of Au^{3+} ions ($KAuCl_4$) to bulk metal resulted in an increase in the size and sensitivity of AuNPs (Fig. 2) [15, 57, 58].

Additionally, size increase can occur through the formation of aggregation. Bioconjugation of AuNPs with complementary oligonucleotide chains results in the formation of AuNP aggregates [16, 59]. In this design, one set of AuNPs is associated with the amplification probe, while another group is associated with the complementing and detecting probes. Amplification and complementary probes hybridize to generate AuNP aggregates that are caught on the T-line and C-line.

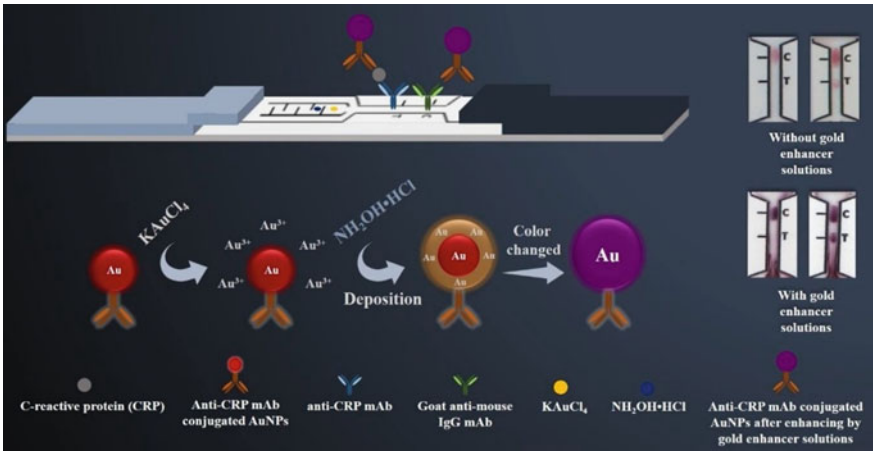

Fig. 2 Automatic sensitivity enhancement using $KAuCl_4$ and $NH_2OH \cdot HCl$. Reprinted from [15], with permission from Elsevier

Incorporation of chemiluminescence with colorimetric method is another strategy for enhancement of sensitivity which is done by modification of AuNPs with horseradish peroxidase (HRP) and antibody which enable chemiluminescence and colorimetric by reaction of luminol [17] and chromogenic agents including TMB (3,3,5,5-tetramethylbenzidine), AEC (3-amino-9-ethylcarbazole) [60, 61]. Moreover, some nanoparticles such as platinum (Pt) nanowires on AuNPs, can successfully replicate the enzymatic actions on the chromogenic agents, leading to an increase in sensitivity and color on the T-line and C-line [42]. In another strategy, after the formation of red color on the T-line and C-line, silver deposition on the gold nanoparticles lead to the formation of black color resulting in enhancement of sensitivity [18]. In a similar manner, polymeric materials such as polydopamine (PDA) can be polymerized onto the AuNPs, which has the benefits of high color intensity and sensitivity, rapid strip detection, and biocompatibility [19]. In order to improve the sensitivity, the decoration of nanosheets or nanoparticles with AuNPs such as graphite-like carbon nitride (g-C_3N_4) with high surface area, was also performed [29, 62].

Integration of strips with a screen-printed electrode (SPE) covered with bioreceptors on the working electrode portion permits LFA with electrochemical readout. In this configuration, AuNPs may transport redox markers such as ferrocene [20]. Occasionally, simple electrochemical LFA strips may be constructed without the addition of redox-active spices. Current may be lowered in this design by trapping AuNPs-antibody conjugates on the detecting zone, which is the working electrode [21]. In another design, Srisomwat et al. synergically used the advantage of automation, delaying architecture, and electrochemical-based LFA [22]. In this design, following the migration of hepatitis B virus (HBV) DNA down to the T-line and capture by the DNA strand on the T-line, Au^{3+} ions are delivered through a baffle barrier with a delayed rate and captured on the hybridized DNA strands via electrostatic and coordination interactions with the phosphate backbone. Subsequently, an anodic stripping voltammetry (ASWV) test was conducted, and the synthesis of AuNPs resulted in the development of a signal owing to the decrease of Au^0.

In addition to some advantages of AuNPs such as excellent electrochemical behavior, high surface area, and considerable biocompatibility, due to their small size and faster migration, single-step electrochemiluminescence (ECL) procedure with mixing tripropylamine as the ECL coreactant with the sample solution can be performed. Benefiting from this, labeling AuNPs with $Ru(bpy)_3^{2+}$ enables the formation of sandwich immunocomplexes at the T-line, which generates an ECL signal in the presence of a $Ru(bpy)_3^{2+}$/tripropylamine (TPA) system (Fig. 3) [23].

2.1.1 Critical Note

Although LFIA strips with naked eye readout have been developed most frequently as the most popular POC device in the diagnosis process, their application may be limited by disadvantages such as qualitative detection, low sensitivity, instability of antibodies, and possible aggregation of AuNPs in serum matrices. Some improvements have been made to improve the sensitivity in an effort to resolve the issues.

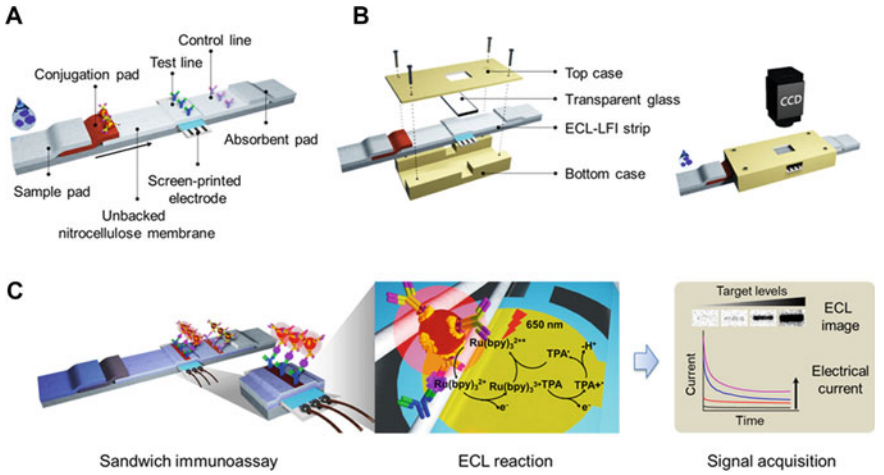

Fig. 3 Application $Ru(bpy)_3^{2+}$-AuNP-Ab for ECL-based LFA: **a** LFA strips structure; **b** assembling the ECL equipment on LFA strip; **c** mechanism of signal producing. Reprinted from [23], with permission from The American Chemical Society

Several amplification strategies, such as deposition of Au, application of two different sizes of AuNPs, and application of AuNPs aggregates, may appear more complicated than the conventional simple LFA method, but they can be executed in a single stage with greater sensitivity than the conventional method.

Another proposed amplification technique involves surrounding AuNPs with HRP in order to perform a chemiluminescence readout. Despite its high sensitivity, this technique may be limited by a time-consuming procedure, the need for a specific reaction temperature (37 °C), and the instability of enzymes. Therefore, alternatives to enzymes such as Pt nanoparticles are advantageous [63]. Although other techniques that increase the color and visibility of T-line and C-line using silver deposition [18] and polymeric materials [19] can be a valuable alternative to the time-consuming enzymatic technique, LFA production can be made affordable by reducing the number of antibodies required. Distribution of AuNPs on a large surface area increases the signal and sensitivity, but the formation of a large nanocomposite reduces the flow rate along the strip and lengthens the testing time, which may limit the performance of this strategy and the use of membranes with small pore sizes that increase sensitivity.

The incorporation of electrochemical approach with LFA has biocompatibility, affordability, compactness, and downsizing capabilities that are more suitable for POC objectives than optical techniques. This idea is implementable on a miniaturized platform containing a small potentiostat, allowing for quick and on-site detection. Due to their exceptional electrochemical properties, AuNPs may be useful in the development of LFAs based on the electrochemical method. However, certain designs, such as ECL-based LFA, can separate LFA technology from POC objectives. Although this technology combines the benefits of AuNPs with ECL in a synergistic

manner, the installation of certain equipment, such as a charge-coupled device (CCD) camera, may raise the cost of the system and restrict its applicability. In addition, for one-step performance and automation of the detection method on the strip, a wax-printing technique is used to create a baffle or zigzag delayed channel. In this method, merging in the non-delayed flow adjusts the transmission of an enhancement reagent such as Au^{3+} to the detecting zone via delayed and non-delayed channels [15, 22]. This design has a high sensitivity and a low LOD, but its complexity and the oxidation of the Au ions may restrict its use.

2.2 Carbon-Based Nanomaterials

Recently, carbon-based nanoparticles such as carbon nanotubes (CNTs), graphene oxide (GO), and carbon dots (CDs) have been widely used in the design of LFA strips due to their high contrast and dark color, low cost, high safety, simple functionalization, portability, and excellent optical and electrochemical properties. The aforementioned benefits are in accordance with the fabrication of POC systems that aim for immediate, inexpensive, and on-site detection of biological targets such as viruses, proteins, DNA, etc., on a compact and portable platform [64]. Compared to AuNPs, CNTs have a greater surface area with high binding sites that are easily functionalized by bioreceptors, resulting in an increased sensitivity. In addition, because of the high contrast between black and white of CTNs, semi-quantification detection may be performed with the naked eye or quantification detection can be conducted during image processing using gray pixels [24]. In a research using CNTs-labeled antibodies for methamphetamine detection, the sensitivity was determined to be 10 times higher than AuNPs-labeled antibodies [24]. CNTs can also be adorned with AuNPs for the immobilization of antibodies, which combines the benefits of both materials [25]. G-C3N4, a two-dimensional (2D) nanomaterial with chemical inertness, a large surface area, and an inexpensive manufacturing technique, is a strong choice for transporting AuNPs (Fig. 4) [29]. Amorphous carbon nanoparticles (ANPs) are unusual nanomaterials with a size greater than 100 nm and a variety of single- and multi-walled CNTs (MWCNTs). ANPs have benefits such as greater sensitivity creation in comparison to AuNPs, non-toxicity, exceptional stability, simple functioning and conjugation, and excellent contrast in comparison to bright backdrops due to their deep black color. The aforementioned characteristics render ANPs appropriate for use as label antibodies in the manufacture of LFA strips [26]. CDs, as carbon-based nanomaterials, are zero-dimensional nanoparticles that possess biocompatibility, low toxicity, inertness, and photostability. These functions employ CDs commonly in drug delivery [65], imaging [66], biosensor [67], and photocatalyst [68]. Thus, the application of CDs as labels of antibodies may be utilized for LFA technique [69]. In this way, hybridization of CDs with other nanoparticles such as SiO_2 might be a useful label for LFA, since it results in great sensitivity for the LFA approach due to its high stability and considerable fluorescence intensity [69].

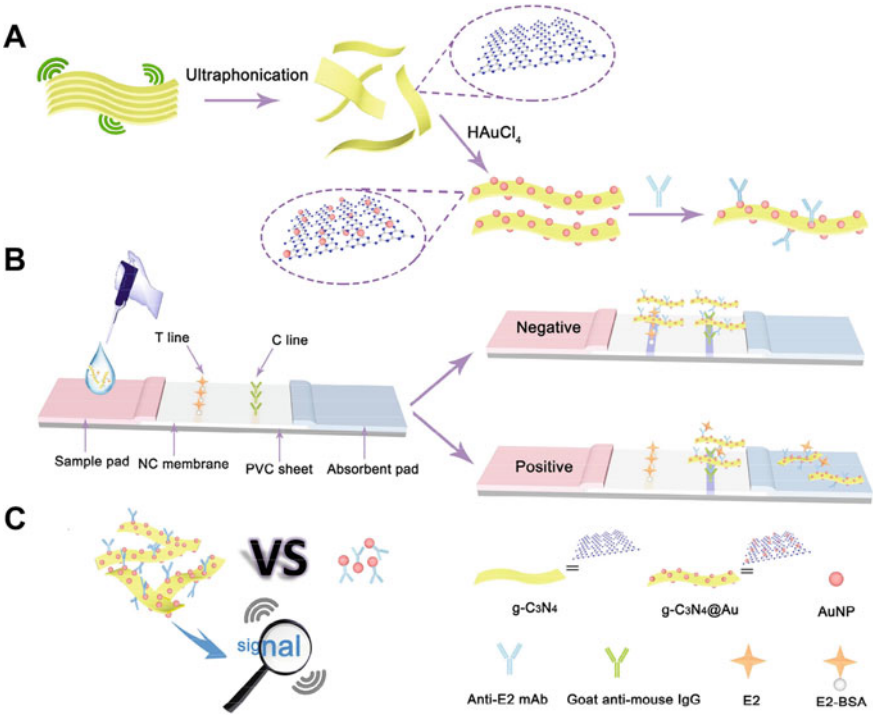

Fig. 4 Application of g-C_3N_4 in LFA: **a** synthesis protocol; **b** detection procedure; **c** enhancement of signal. Reprinted from [29], with permission from Elsevier

Benefiting from the FRET effect of CDs fluorescence intensity with certain quencher nanoparticles, such as silver nanoparticles (AgNPs), substantial absorption at the CDs fluorescence emission wavelength may occur. Li et al. constructed a strip in this manner by immobilizing a combination of zearalenone-ovalbumin and CD-ovalbumin on the T-line and zearalenone-ovalbumin on the C-line. In this configuration, AgNPs-anti-zearalenone served as the acceptor (quencher) while CD-ovalbumin served as the donor [27]. In addition to enhancing the optical characteristics of CNTs, their high conductivity also allows them to be employed as the working electrode. Zue et al. developed a concept for LFA employing CNT paper on the C-line and Ag/AgCl ink-painted copper paper as the reference/counter electrode, followed by lamination of the strip. In this approach, BSA–8-hydroxyguanosine on the T-line collected AuNP–anti–8-hydroxyguanosine conjugates. The AuNP–anti–8-hydroxyguanosine/8-hydroxyguanosine complexes then moved across the T-line and were caught by anti-Mouse IgG on the C-line, resulting in the detection of the antigen [21]. CNT-modified screen-printed carbon electrode (SPE) that is mounted under the T-line using a magnet is a second design option [28]. This structure was designed to

evaluate the enzymatic activity of acetylcholinesterase (AChE) for acetylthiocholine (ATCh) by comparing deactivated AChE to active AChE trapped by anti-AChE on the T-line.

2.2.1 Critical Note

Due to the insolubility of CNT in sample buffers and the slow migration of CNT in the pores of nitrocellulose, some pre-treatment such as oxidation or surfactant binding must be performed before CNTs may be linked to multiple bioreceptors [24]. In addition, CNT modification of the electrode is heavily dependent on organic solvents for effective dispersion. For LFA strips, the suggested nanoparticles with high solubility, such as CDs, and the benefits of easy functionalization, simple synthesis, high safety, low cost, and high quantum yield in solid and aqueous phases are viable candidates. Some developments, such as the inclusion of CDs with other nanoparticles such as SiO_2, result in the non-uniformity of this kind of nanoparticles due to the co-hydrolysis of CDs and tetraethyl orthosilicate (TEOS) [69]. Although designing FRET-based LFA strips enables on-site screening of targets in complex matrices, such as zearalenone in cereal samples and relevant products, the qualitative, semi-quantitative, and probable interferences of matrices may limit the scope of this method's use [27].

2.3 Quantum Dots (QDs)

QDs as semiconductor nanoparticles are typically a mix of elemental groups III–V and II–VI. Due to the quantum confinement of electrons and holes in these nanoparticles, continuous molecular band energy is converted to discrete energy levels, resulting in the potential emission of fluorescence upon excitation and electron-hole recombination. QDs with advantages of controllable size-depended emission, high specific surface area, high fluorescence intensity, long lifetime, high binding sites, wide absorption region, low photodegradation, and photo-bleaching, have been widely used for designing biosensors in comparison with other organic commercial dyes [70]. Due to the aforementioned characteristics, QDs have attracted considerable interest for the creation of LFA strips to detect proteins [71], viruses [72], pharmaceutical materials [73], and nucleic acid [74]. Although QDs indicate a high level of sensitivity to the LFA system, it is possible to process some technologies to increase sensitivity. Due to the formation of hydrophilic QDs in the presence of thiolated acids, an abundance of carboxylic acids can coat the surface, facilitating the immobilization of amino-terminated aptamers and DNAs. Thus, CdTe QDs were combined with strand displacement amplification method for HIV-DNA detection. This approach conducted by hybridization of hairpin H1-strand as a trigger, with HIV-DNA leading to unraveling the hairpin structure of H1. Thus, the remaining H1 strand can hybridize with the CdTe hairpin H2 strand that has been tagged with

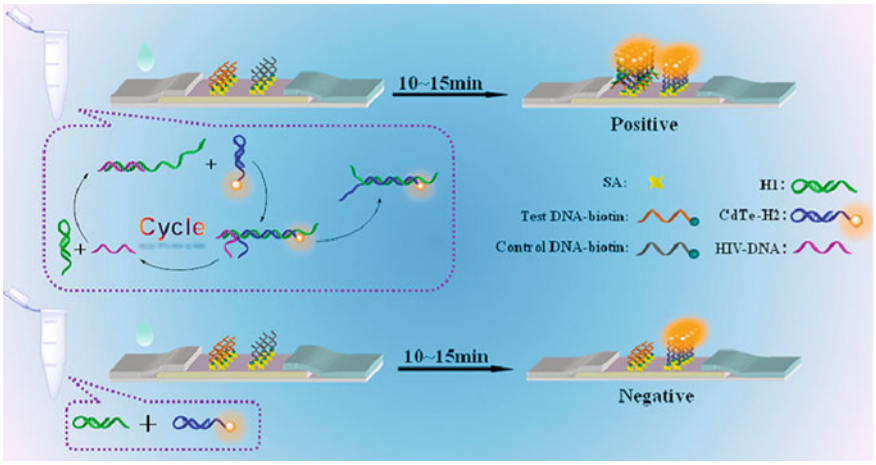

Fig. 5 Strand displacement amplification-based LFA for detection of HIV-DNA. Reprinted from [30], with permission from Elsevier

QDs, followed by the release of HIV-DNA. As seen in Fig. 5, this circle may be repeated and an amplification sample can be deposited onto the sample pad. Finally, H1–H2-CdTe QDs hybridization was captured on the T-line by the unhybridized H2 strand sequence [30].

The employment of core/shell QDs is advised for enhancing the sensitivity of QDs-based LAF techniques. So, CdSe/ZnS QDs are extensively employed in the creation of biosensors, particularly, LFA strips [31]. In this method, core/shell QDs may be constructed via multishell strategy to increase the quantum yield and sensitivity of LFA technology. By preventing exciton leakage, the surrounding ZnSe/CdSe core with a CdS/Cd_xZn_{1-x}S/ZnS multishell may significantly increase the quantum yield to 70% [32]. $CuInZn_xS_{2+x}$ ($x = 1$) as a cadmium-free core is capped by ZnS/ZnS as a thick shell, which is synthesized during two independent shell growth processes for the purpose of multishell development in LFA. This structure can provide a 77% quantum yield [33]. In order to generate cadmium-free and environmentally acceptable QDs, InP/ZnS core/shell QDs were encased in a silica shell for LFA design [75]. QD/SiO_2 nanoparticles including dendritic and porous silica particles with densely loaded CdSe/CdS/ZnS QDs were proposed for creating LFA strips [34]. Compared to typical sandwich-type nanospheres, in which a layer of fluorophores surrounding the silica core, this shape significantly increases the surface area for adsorption of QDs and makes homogenous dispersion of QDs throughout the silicon sphere practical. The accumulation of QDs in each unity led to outstanding optical properties, colloidal stability, and simple biofunctionalization of the suggested nanoparticle. The inclusion of beforementioned properties with LFA strips led to the establishment of a powerful platform for the detection of C-reaction protein (CRP) in complicated biological samples [34]. For enhancement of the sensitivity, adsorption of QDs on the surface of biocompatible nanobeads with large surface area is another approach.

Shao et al. produced nanobeads (Fig. 6) using sodium dodecyl sulfonate (SDS) and poly (maleicanhydride-alt-1-octadecene) (PMAO) for this purpose, which were subsequently coated with CdSe/ZnS QDs [35].

The readout signals from QDs-based LFA can be performed by UV light followed by an assessment of intensities using ImageJ application or by fluorescence strip reader. Signaling from QDs-based LFA can be accomplished by directly emitted fluorescence intensity of QDs-labeled bioreceptors or measurement of QDs intensity quenching. LFA strips can be produced by quenching emitting antigen-linked QDs on the T-line with antibody-linked AgNPs or AuNPs utilizing an inner filter and fluorescence resonance energy transfer (FRET), respectively [31]. Also, a nanocomposite of quantum dots (Biotin-QDs) and MnO_2 nanosheets, which results in the

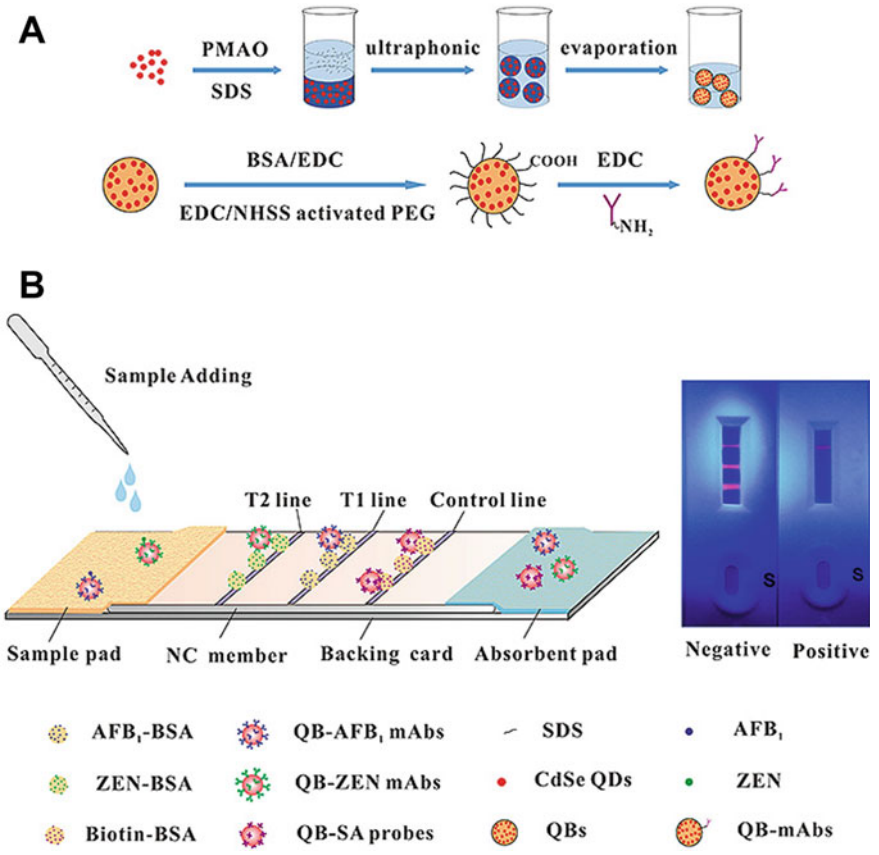

Fig. 6 Application quantum dot nanobeads (QBs) for multiplexed-LFA detection of aflatoxin B1 (AFB1) and zearalenone (ZEN); **a** synthesis protocol; **b** detection process. Reprinted from Analytica Chimica Acta, Vol. 1025, Shao et al., Quantum dot nanobead-based multiplexed immunochromatographic assay for simultaneous detection of aflatoxin B1 and zearalenone, Pages 163–171, Copyright 2018, with permission from Elsevier [35]

quenching of QDs, can be used as a decoration for QDs. MnO_2 nanosheets are degraded in the presence of glutathione (GSH), allowing Biotin-QDs to be collected on a streptavidin-containing T-line [76].

2.3.1 Critical Note

Compared to typical AuNPs, QDs have a greater specific surface area, acceptable biocompatibility, increased sensitivity, quicker strip migration, and simple storage conditions. Furthermore, the simple binding of QDs to nucleic acid strands enables the performance of displacement amplification technology, which introduced a potent method that, in comparison to conventional methods such as loop-mediated isothermal amplification (LAMP), recombinase polymerase amplification (RPA), and polymerase chain reaction (PCR), is easier to operate, does not require expensive biological material, and does not necessitate expert knowledge [30]. Due to the application of the synthesis technique in an organic phase, the stability and quantum yield of core/shell QDs might be diminished after transfer to a biological aqueous environment, hence affecting the sensitivity of the LFA system [33]. In addition, QDs-based LFAs are hampered by issues such as high toxicity of heavy metal elements, limited stability, aggregation in biological samples, and a quenching effect in the presence of biomolecules.

2.4 Magnetic Nanoparticles (MNPs)

Typically, these nanoparticles are produced using iron oxide nanoparticles (Fe_3O_4, γ-Fe_2O_3) as a foundation core, which is then coated with additional nanoparticles and bioreceptors are immobilized. This property enables the construction of core/shell structures for the application of LFA, such as Fe_2O_3 nanoparticles containing gold [36], SiO_2 [37], streptavidin [38], and protein G [39]. In addition, because of their large surface area and simple carboxyl group functionalization, Fe_2O_3 nanoparticles can be directly linked to antibodies [40] or other bioreceptors. The primary flaw of conventional MNPs is aggregation during migration along strips, which slows down the detection process and reduces sensitivity owing to weaker antigen–antibody interactions. Super-paramagnetic nanoparticles (SPMNPs) with a larger surface area and no hysteresis have been shown to be an effective solution to this issue. SPMNPs are ascribed to MNPs less than 20 nm in size. Furthermore, MNPs having a size between 30 and 100 nm are paramagnetic [1]. Wang et al. demonstrated the size of SPMNPs has a substantial impact on the detection time [77]. Different magnetometers, such as resonant coil [78], magnetoresistance [79], and planar coils [80], can read the signal of MNPs. Magnetometers are installed above the detecting zone of the strips for this purpose, as the existence of an external magnetic field is crucial for the emergence of the magnetization effect of MNPs [81]. Due to the obvious brown color of Fe_2O_3 or their coating by AuNPs, T-line and C-line can be read with the naked eye (Fig. 7) [36,

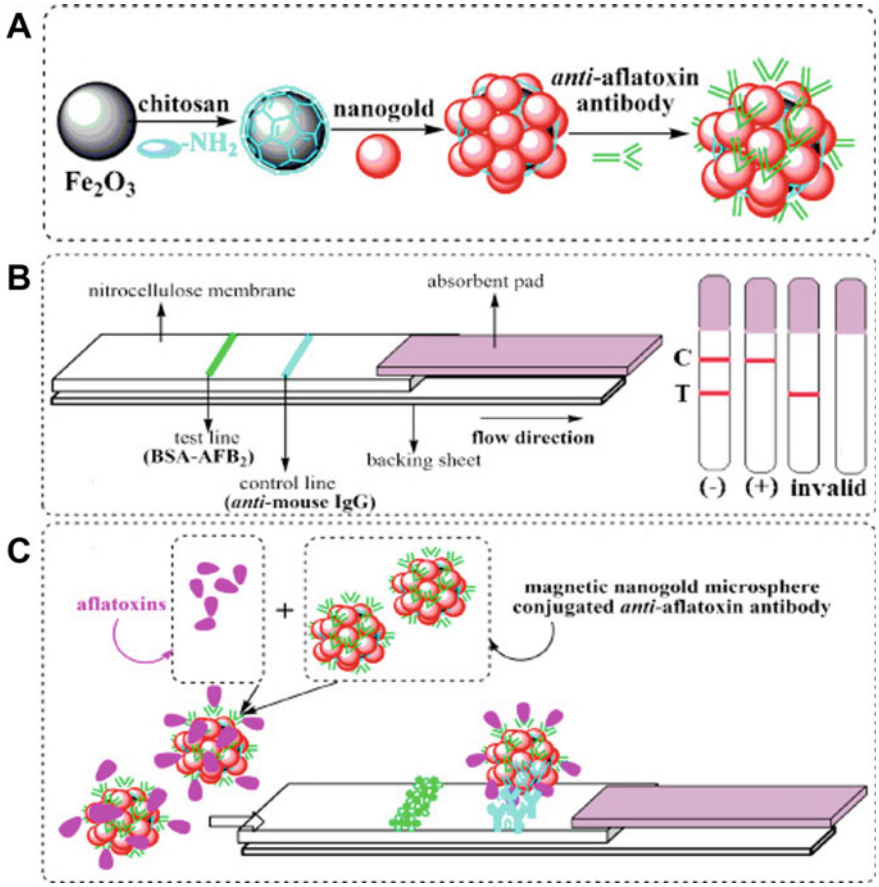

Fig. 7 Application of Fe_2O_3–AuNPs-antibody for detection of aflatoxin B_2. Reprinted from [36], with permission from Elsevier

39]. Incorporation of Fe_2O_3 nanoparticles with LFA can be allocated to the sample preparation prior to its placement on the sample pad, extending their use beyond signal creation. Li et al. implemented magnetic enrichment of *L. monocytogenes* cells from lettuce by streptavidin-biotin interaction, DNA extraction, and detection by AuNP-probe on LFA strip [38].

2.4.1 Critical Note

In comparison to fluorophore nanoparticles, MNPs have the benefits of reduced background, the need for inexpensive, compact, and compact magnetometers, and make on-site and downsized POC detection possible. Furthermore, movement along the strips is navigable utilizing an external magnetic field. Due to limited solubility

and dispersion in water, the use of these nanoparticles may be challenging despite the fact that these characteristics might provide the MNPs-based LFA more credit than other types of LFAs that need expensive and large equipment. In addition, size-dependent issues can be attributed to aggregation and positive errors caused by MNPs of greater sizes, or to poor magnetic signal and low sensitivity caused by MNPs of lower sizes [77]. Another difficulty is the two-step growth of the output signal with time, which may be regulated by the kinetics of immunoreaction [82].

2.5 Nanoenzymes

As a result of the incorporation of natural enzymes with LFA, the signal strength of the redox reaction of chromogenic substrates-H_2O_2 system on the detecting zone may have increased, resulting in visible color. In addition to colorimetry, LFA can also contain chemiluminescence owing to the benefits of nanoenzymes. This technique is typically carried out by trapping horseradish peroxidase (HRP)-labeled antibody on the T-line or C-line, followed by the addition of chromogenic substrates such as TMB (3,30,5,50-tetramethylbenzidine) and ABTS (20-azino-bis(3-ethylbenzothiazole-6-sulfonic acid) [52, 83]. Additionally, G-quadruplexe-hemin DNAzyme has enzymatic effects, but it has been utilized less frequently for LFA. This process often has a number of drawbacks, including particular requirements such as temperature (37 °C), buffer, and expense. Recently, nanoenzymes have attracted the interest of scientists for the creation of LFAs due to their remarkable properties, which include enzyme function mimicry, low cost, ease of manufacture, and increased stability [84]. In this manner, nanoenzymes having peroxidase activity, such as nanoparticles based on platinum (Pt), have been widely utilized in the construction of LFAs. The regular inclusion of nanoenzymes with LFAs has advanced based on the coating of AuNPs with Pt layer [41] or Pt nanowires [42], porous Pt layer [43], which boosts the plasmonic color of AuNPs by adding chromogenic substrate to the detecting zone (Fig. 8). In certain instances, palladium-platinum (Pd–Pt) nanoparticles were produced for LFA design [44].

2.5.1 Critical Note

Application of nanoenzymes in LFA has benefits such as low cost, high stability, and simple preparation, but detection requires the addition of chromogenic substrate to the detecting zone to generate a readable signal, which makes the procedure tedious and time-consuming. Although certain innovations, such as automating the technique by coating and drying the strips with chromogenic substrate, can speed up the detection, constructing the strips with additional channels for the separate migration of chromogenic substrate in the sample solution might complicate the LFA procedure [85].

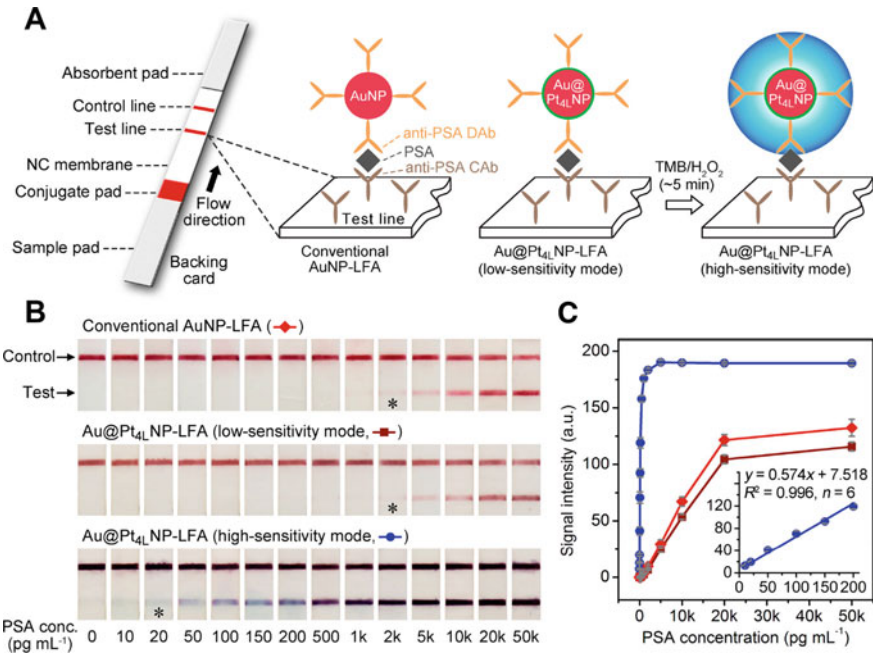

Fig. 8 Catalytic effect of Au@Pt-antibody for TMB/H_2O_2 and enhancement of sensitivity. The sign of (*) shows LOD. Reprinted from [41], with permission from The American Chemical Society

2.6 Other Nanoparticles

Nanoparticles have been widely utilized in the structuring of LFA strips. However, there have been other key nanoparticles that have been less integrated with LFA and have synergistically shared their properties with LFA to permit the high sensitivity and accuracy necessary for POC techniques. These nanoparticles are mentioned and briefly described in the next section. Upconversion nanoparticles (UCNPs) capable of photon upconversion are created by doping transition metals with actinides and lanthanides derived from rare earths. UCNPs are able to absorb a large number of photons from the low-energy near-infrared (NIR) region and convert them into a single photon from the high-energy ultraviolet-visible range (UV-Vis). Scientists are more interested in the application of UCNPs in nanomedicine, biosensors, and in vivo imaging than QDs due to their narrow and high-intensity emission, reduced toxicity, anti-Stokes shifts, high cellular uptake, low background, and strong optical penetration in tissue [86]. $NaYF_4$ double-doped with Yb and Er has been the most often included UCNPs with LFA ($NaYF_4$: Yb, Er). In this system, the matrix with the lowest phonon energy is $NaYF_4$. Also, Yb^{3+} is able to absorb an infrared photon in the host lattice, which is then transmitted to the non-radiative form of Er^{3+}, which transforms it into visible emission [87]. Moreover, in order to enhance the intensity and sensitivity of $NaYF_4$ UCNPs, several modifications might be made [45]. Doping

the Ca^{2+} ions in the shell of $NaYF_4$:Yb, Tm@$NaYF_4$ core/shell UCNPs in this manner can enhance the NIR emission via excitation in the NIR region. This event can occur as a result of lattice destruction followed by the formation of an asymmetric structure driven by the displacement of Y^{3+} with Ca^{2+}, resulting in a highly sensitive electron transition (Fig. 9).

Time-resolved fluorescence nanoparticles (TRFNPs) are fluorescent lanthanide (mostly Europium (III)) chelates nanoparticles with a hydrophobic shell that must be modified with biofunctional groups [88]. With their extended lifetime, chemical stability, large Stokes shift, and broad excitation spectrum, these nanoparticles

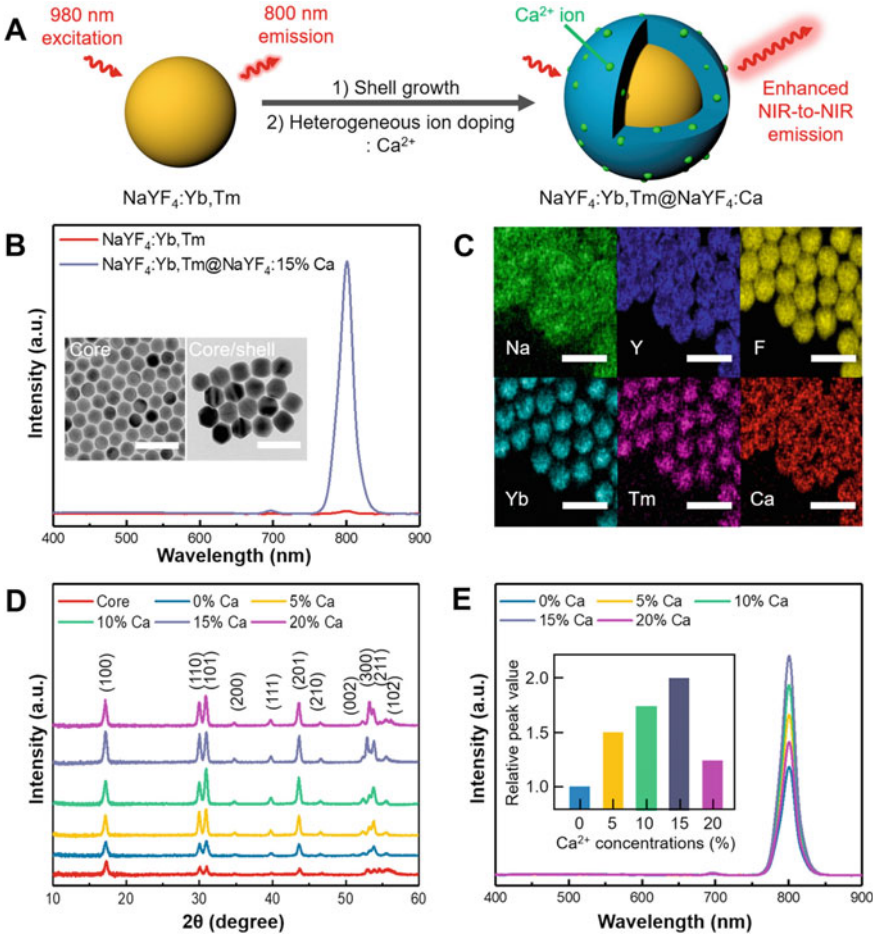

Fig. 9 NIR-to-NIR $NaYF_4$:Yb, Tm@$NaYF_4$@ Ca^{2+} UCNPs: **a** schematic illustration of synthesis; **b** enhancement of fluorescence intensity by $NaYF_4$ shell and Ca^{2+} dopant; **c** elemental mapping; **d** XRD spectra; **e** effect of different amount of Ca^{2+} dopant on the fluorescence intensity. Reprinted from [45], with permission from Elsevier

significantly minimize interferences in biological and complex matrices with transient background. Therefore, TRFNPs may be suitable for integration with LFA [46]. Surface-enhanced Raman scattering (SERS) nanotags are plasmonic metal nanostructures, such as gold and silver, that enable the detection of targets adsorbed on their surface via Raman signal enhancement resulting from electromagnetic field amplification via localized surface plasmon resonance (LSPR) by hot spot effect [89]. This occurrence can be attributed to the increase of the electromagnetic field caused by plasmonic phenomena (Stock, Rayleigh, Anti-Stocks) that lead to SERS in nanoscale gaps between nanostructures [52]. Increased Raman intensity at a constant Raman shift is used for detection (cm^{-1}). In this method, He–Ne laser (365 nm) or Raman (diode) laser (785 nm) is often utilized as the excitation source, and a holographic notch filter is employed to remove the Rayleigh line from the Raman data [47, 50]. Several nanoparticles, including hollow gold nanospheres [47], Au nanoflower @ Ag core/shell [48], Au@Ag nanoparticles [49], Au nanorod (AuNR)@ Au core/shell, have been combined with LFA in this manner [50]. Raman molecules such as malachite green isothiocyanate (MGITC) [47], 4-mercaptobenzoic acid (MBA) [48], 1,4-nitrobenzenthiole (NBT) [50] and 5,5′-dithiobis-(2-nitrobenzoic acid) (DTNB) [49] have been embedded or adsorbed in nanoparticles in order to produce Raman intensity. The fabrication of Au@Ag nanoparticles with dual-layer DTNB is depicted in Fig. 10.

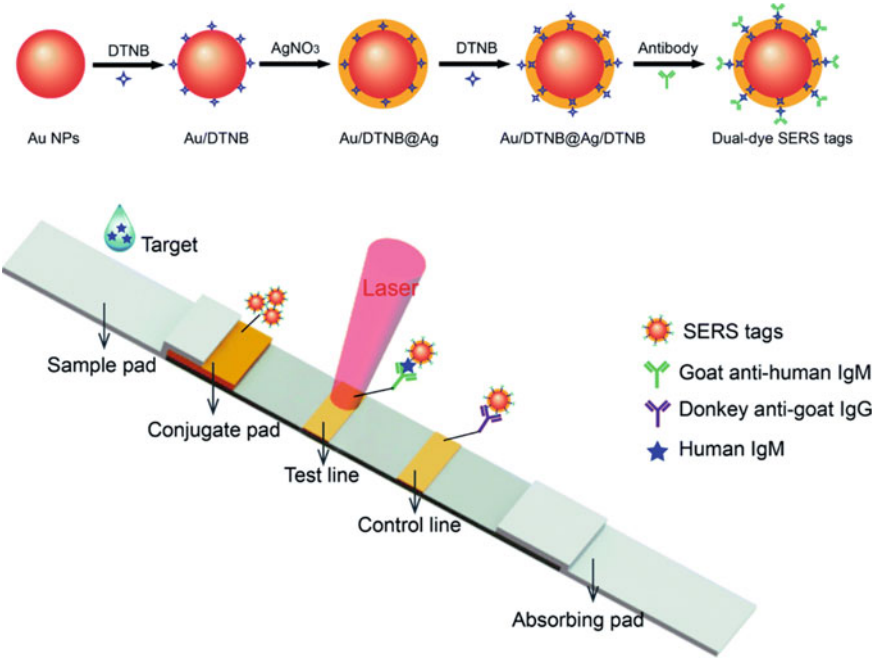

Fig. 10 Preparation and application of Au@DTNB@Ag@DTNB in LFA. Adapted from [49], in accordance with the Creative Commons Attribution 3.0 Unported Licence (CC BY)

2.6.1 Critical Note

The aforementioned nanoparticles serve an indisputable effect in reducing interferences from the background. The UCPs and SERS-nanotags with anti-Stokes or Stokes shifts induced by NIR excitation and UV-Vis or NIR emission significantly reduce the autofluorescence of UV-Vis region-absorbent biomolecules. Also, TRFNPs with extended lifetime fluorescence relative to interferences' short-lived fluorescence may be combined with LFA. Despite these advantages, their applicability may be limited by some downsides. The creation of UCNPs necessitated the use of inert gas (N_2, Ar) or vacuum, which are costly conditions that are available in all laboratories. Due to the poor solubility of UCNPs, migration along strips may also be challenging. Therefore, alteration and surface functionalization are essential. For capturing the signal of TRFNPs over their lifetime, time-resolving techniques, which are not standard on all spectrometers and are costly, are required. Despite the fact that SERS-nanotags improve the limited sensitivity caused by weak signals in the NIR window [90], this technology requires the use of costly commercial Raman molecules in nanoparticles. In contrast, even though the SERS approach attempts to minimize interferences by the use of NIR lasers and stock spectra, some background signal interferences from nanotags may still be present. In order to further limit interferences, the synthesis of very homogeneous nanoparticles may thereby complicate the synthesis technique.

3 Conclusion

The primary objective of point-of-care (POC) devices is to provide rapid, cost-effective, and accurate diagnosis of targets in a variety of domains, including medical, criminal, clinical, and industrial, in order to avoid and forecast potential issues and aid in prompt treatment. One of the most intriguing elements of POC devices is the development of in-home, patient-centered screening and healthcare diagnostics. As an accessible and simple-to-prepare POC gadget, LFA has become a popular diagnostic tool. Nanomaterials, which are an integral part of the LFA methodology, have played a crucial role in the effective design and execution of this method to increase its sensitivity. Nanomaterials have unique benefits, such as adjustable physical and chemical properties based on size, shape, and composition and simple functionalization using bioreceptors combined with LFA. According to the findings given in Table 1, production, modification, and bioconjugation of nanoparticles well-incorporated with LFA strips for the detection of diverse targets include biomarkers, viruses, microorganisms, DNA, mycotoxins, etc. As demonstrated in Table 1, the detection of targets has occurred in less than 30 min, suggesting an adequate rate of diagnosis due to the absence of aggregation, the rapid migration through membrane pores, and the successful interpretation of the signal created by nanoparticles. AuNPs have been the most prevalent and popular nanoparticles that enable naked-eye detection of T-line or C-line. Unfortunately, the typical LFA based on naked-eye qualifying detection has a

limited detection. In addition, certain image analysis software is essential for quantifying data, which makes the measurement challenging. So, to increase sensitivity, the integration of alternative transduction systems with LFA using other nanoparticles has been encouraged. In this context, CNTs with vibrant colors and a strong black-on-white contrast may be suitable for inclusion with LFA. Due to the poor dispersity and hydrophilicity of the migration buffer, however, CNTs are not commonly included with commercially available LFA. In addition, the use of carbon-based nanoparticles for electrochemically-based LFA is in great demand for SPE, making this technology extremely costly. On the other hand, despite the fact that the use of other nanoparticles benefits from the high sensitivity of QDs, the miniaturized magnetometer for MNPs, and the significant reduction of interference by UCNPs and SERS-nanotags, the readout of signals requires the integration of costly equipment with LFA. This issue prohibits personalized detection and in-home use of LFA, which contradicts the objectives of the POC approach. The catalytic impact of nanoenzymes on substrates, accompanied by an increase in sensitivity and a reduction in LOD (10^3 times) [41], can be a valuable alternative to the usual LFA approach for detection with the naked eye. In addition, the design of delayed canals for the automation of LFA may be suitable for commercialization [15].

Acknowledgements A. M. and G. A. gratefully acknowledge Mashhad University of Medical Sciences, Iran for supporting this study. Y.N.E. acknowledges funding support from the 2232 International Fellowship for Outstanding Researchers Program of TÜBİTAK (Project No: 118C346).

References

1. Mohammadinejad A et al (2022) Development of lateral flow assays for rapid detection of troponin I: a review. Crit Rev Anal Chem 1–15
2. Khandan-Nasab N et al (2021) Biosensors, microfluidics systems and lateral flow assays for circulating microRNA detection: a review. Anal Biochem 633:114406
3. Napione L (2021) Integrated nanomaterials and nanotechnologies in lateral flow tests for personalized medicine applications. Nanomaterials 11(9):2362
4. Quesada-González D, Merkoçi A (2015) Nanoparticle-based lateral flow biosensors. Biosens Bioelectron 73:47–63
5. de Puig H et al (2017) Challenges of the nano-bio interface in lateral flow and dipstick immunoassays. Trends Biotechnol 35(12):1169–1180
6. Holzinger M, Le Goff A, Cosnier S (2014) Nanomaterials for biosensing applications: a review. Front Chem 2:63
7. SadAbadi H et al (2013) Integration of gold nanoparticles in PDMS microfluidics for lab-on-a-chip plasmonic biosensing of growth hormones. Biosens Bioelectron 44:77–84
8. Hibbard T et al (2013) Point of care monitoring of hemodialysis patients with a breath ammonia measurement device based on printed polyaniline nanoparticle sensors. Anal Chem 85(24):12158–12165
9. Wang S et al (2013) Point-of-care assays for tuberculosis: role of nanotechnology/microfluidics. Biotechnol Adv 31(4):438–449
10. Janegitz BC, Cancino J, Zucolotto V (2014) Disposable biosensors for clinical diagnosis. J Nanosci Nanotechnol 14(1):378–389

11. Medina-Sánchez M, Miserere S, Merkoçi A (2012) Nanomaterials and lab-on-a-chip technologies. Lab Chip 12(11):1932–1943
12. de la Escosura-Muñiz A, Merkoçi A (2010) Electrochemical detection of proteins using nanoparticles: applications to diagnostics. Expert Opin Med Diagn 4(1):21–37
13. Mahmood A, Khan SU-D, Rehman F (2015) Assessing the quantum mechanical level of theory for prediction of UV/Visible absorption spectra of some aminoazobenzene dyes. J Saudi Chem Soc 19(4):436–441
14. Choi DH et al (2010) A dual gold nanoparticle conjugate-based lateral flow assay (LFA) method for the analysis of troponin I. Biosens Bioelectron 25(8):1999–2002
15. Panraksa Y et al (2021) A facile one-step gold nanoparticles enhancement based on sequential patterned lateral flow immunoassay device for C-reactive protein detection. Sens Actuators B Chem 329:129241
16. Hu J et al (2013) Oligonucleotide-linked gold nanoparticle aggregates for enhanced sensitivity in lateral flow assays. Lab Chip 13(22):4352–4357
17. Chen Y et al (2016) A dual-readout chemiluminescent-gold lateral flow test for multiplex and ultrasensitive detection of disease biomarkers in real samples. Nanoscale 8(33):15205–15212
18. Anfossi L et al (2013) Increased sensitivity of lateral flow immunoassay for ochratoxin A through silver enhancement. Anal Bioanal Chem 405(30):9859–9867
19. Xu S et al (2019) Lateral flow immunoassay based on polydopamine-coated gold nanoparticles for the sensitive detection of zearalenone in maize. ACS Appl Mater Interfaces 11(34):31283–31290
20. Sinawang PD et al (2016) Electrochemical lateral flow immunosensor for detection and quantification of dengue NS1 protein. Biosens Bioelectron 77:400–408
21. Zhu X et al (2014) A paper electrode integrated lateral flow immunosensor for quantitative analysis of oxidative stress induced DNA damage. Analyst 139(11):2850–2857
22. Srisomwat C et al (2020) Amplification-free DNA sensor for the one-step detection of the hepatitis B virus using an automated paper-based lateral flow electrochemical device. Anal Chem 93(5):2879–2887
23. Hong D et al (2021) Electrochemiluminescence-incorporated lateral flow immunosensors using Ru (bpy) 32+-labeled gold nanoparticles for the full-range detection of physiological C-reactive protein levels. Anal Chem 93(22):7925–7932
24. Sun W et al (2017) A novel multi-walled carbon nanotube-based antibody conjugate for quantitative and semi-quantitative lateral flow assays. Biosci Biotechnol Biochem 81(10):1874–1882
25. Liu Y et al (2017) Gold nanoparticles decorated carbon nanotube probe based immunochromatographic assay on cotton thread. Sens Actuators B Chem 251:1112–1118
26. Zhang X et al (2017) Multiplex lateral flow immunoassays based on amorphous carbon nanoparticles for detecting three fusarium mycotoxins in maize. J Agric Food Chem 65(36):8063–8071
27. Li S et al (2018) Fluorometric lateral flow immunochromatographic zearalenone assay by exploiting a quencher system composed of carbon dots and silver nanoparticles. Microchim Acta 185(8):1–9
28. Du D et al (2012) Integrated lateral flow test strip with electrochemical sensor for quantification of phosphorylated cholinesterase: biomarker of exposure to organophosphorus agents. Anal Chem 84(3):1380–1385
29. Yao X et al (2021) Graphite-like carbon nitride-laden gold nanoparticles as signal amplification label for highly sensitive lateral flow immunoassay of 17β-estradiol. Food Chem 347:129001
30. Deng X et al (2018) Applying strand displacement amplification to quantum dots-based fluorescent lateral flow assay strips for HIV-DNA detection. Biosens Bioelectron 105:211–217
31. Anfossi L et al (2018) A lateral flow immunoassay for straightforward determination of fumonisin mycotoxins based on the quenching of the fluorescence of CdSe/ZnS quantum dots by gold and silver nanoparticles. Microchim Acta 185:1–10
32. Shen H et al (2011) Phosphine-free synthesis of high-quality reverse type-I ZnSe/CdSe core with CdS/CdxZn1−xS/ZnS multishell nanocrystals and their application for detection of human hepatitis B surface antigen. Nanotechnology 22(37):375602

33. Wu R et al (2018) Synthesis of highly stable CuInZnS/ZnS//ZnS quantum dots with thick shell and its application to quantitative immunoassay. Chem Eng J 348:447–454
34. Huang L et al (2018) Brilliant pitaya-type silica colloids with central–radial and high-density quantum dots incorporation for ultrasensitive fluorescence immunoassays. Adv Func Mater 28(4):1705380
35. Shao Y et al (2018) Quantum dot nanobead-based multiplexed immunochromatographic assay for simultaneous detection of aflatoxin B1 and zearalenone. Anal Chim Acta 1025:163–171
36. Tang D et al (2009) Magnetic nanogold microspheres-based lateral-flow immunodipstick for rapid detection of aflatoxin B2 in food. Biosens Bioelectron 25(2):514–518
37. Zhang X et al (2011) A silicon dioxide modified magnetic nanoparticles–labeled lateral flow strips for HBs antigen. J Biomed Nanotechnol 7(6):776–781
38. Li F et al (2018) Biotin-exposure-based immunomagnetic separation coupled with nucleic acid lateral flow biosensor for visibly detecting viable Listeria monocytogenes. Anal Chim Acta 1017:48–56
39. Ryu Y et al (2011) Increase in the detection sensitivity of a lateral flow assay for a cardiac marker by oriented immobilization of antibody. BioChip J 5:193–198
40. Lu W et al (2017) Dual immunomagnetic nanobeads-based lateral flow test strip for simultaneous quantitative detection of carcinoembryonic antigen and neuron specific enolase. Sci Rep 7(1):1–10
41. Gao Z et al (2017) Platinum-decorated gold nanoparticles with dual functionalities for ultrasensitive colorimetric in vitro diagnostics. Nano Lett 17(9):5572–5579
42. Zhang J et al (2019) Gold-platinum nanoflowers as a label and as an enzyme mimic for use in highly sensitive lateral flow immunoassays: application to detection of rabbit IgG. Microchim Acta 186:1–9
43. Loynachan CN et al (2018) Platinum nanocatalyst amplification: redefining the gold standard for lateral flow immunoassays with ultrabroad dynamic range. ACS Nano 12(1):279–288
44. Han J et al (2018) Nanozyme-based lateral flow assay for the sensitive detection of Escherichia coli O157: H7 in milk. J Dairy Sci 101(7):5770–5779
45. Kim J et al (2018) Rapid and background-free detection of avian influenza virus in opaque sample using NIR-to-NIR upconversion nanoparticle-based lateral flow immunoassay platform. Biosens Bioelectron 112:209–215
46. Huang B et al (2017) A novel time-resolved fluoroimmunoassay for the quantitative detection of antibodies against the phospholipase A2 receptor. Sci Rep 7(1):1–8
47. Hwang J, Lee S, Choo J (2016) Application of a SERS-based lateral flow immunoassay strip for the rapid and sensitive detection of staphylococcal enterotoxin B. Nanoscale 8(22):11418–11425
48. Fu X et al (2017) Ultrasensitive detection of the β-adrenergic agonist brombuterol by a SERS-based lateral flow immunochromatographic assay using flower-like gold-silver core-shell nanoparticles. Microchim Acta 184:1711–1719
49. Jia X et al (2018) Dual dye-loaded Au@ Ag coupled to a lateral flow immunoassay for the accurate and sensitive detection of Mycoplasma pneumoniae infection. RSC Adv 8(38):21243–21251
50. Khlebtsov BN et al (2019) SERS-based lateral flow immunoassay of troponin I by using gap-enhanced Raman tags. Nano Res 12:413–420
51. Nooranian S et al (2022) Biosensors based on aptamer-conjugated gold nanoparticles: a review. Biotechnol Appl Biochem 69(4):1517–1534
52. Mohammadinejad A et al (2020) Development of biosensors for detection of alpha-fetoprotein: as a major biomarker for hepatocellular carcinoma. TrAC, Trends Anal Chem 130:115961
53. Soler M, Huertas CS, Lechuga LM (2019) Label-free plasmonic biosensors for point-of-care diagnostics: a review. Expert Rev Mol Diagn 19(1):71–81
54. Kim DS et al (2016) Development of lateral flow assay based on size-controlled gold nanoparticles for detection of hepatitis B surface antigen. Sensors 16(12):2154
55. Lou S et al (2012) A gold nanoparticle-based immunochromatographic assay: the influence of nanoparticulate size. Analyst 137(5):1174–1181

56. Zhu J et al (2011) Simultaneous detection of high-sensitivity cardiac troponin I and myoglobin by modified sandwich lateral flow immunoassay: proof of principle. Clin Chem 57(12):1732–1738
57. Kim W, Lee S, Jeon S (2018) Enhanced sensitivity of lateral flow immunoassays by using water-soluble nanofibers and silver-enhancement reactions. Sens Actuators B Chem 273:1323–1327
58. áEric Aston D, áLarry Branen A (2012) DNA detection on lateral flow test strips: enhanced signal sensitivity using LNA-conjugated gold nanoparticles. Chem Commun 48(62):7714–7716
59. Ge C et al (2013) An enhanced strip biosensor for rapid and sensitive detection of histone methylation. Anal Chem 85(19):9343–9349
60. Parolo C, de la Escosura-Muñiz A, Merkoçi A (2013) Enhanced lateral flow immunoassay using gold nanoparticles loaded with enzymes. Biosens Bioelectron 40(1):412–416
61. He Y et al (2011) Ultrasensitive nucleic acid biosensor based on enzyme–gold nanoparticle dual label and lateral flow strip biosensor. Biosens Bioelectron 26(5):2018–2024
62. Xu H et al (2014) Gold-nanoparticle-decorated silica nanorods for sensitive visual detection of proteins. Anal Chem 86(15):7351–7359
63. Zhang J et al (2019) Gold-platinum nanoflowers as a label and as an enzyme mimic for use in highly sensitive lateral flow immunoassays: application to detection of rabbit IgG. Microchim Acta 186(6):1–9
64. Justino CI, Rocha-Santos TA, Duarte AC (2013) Advances in point-of-care technologies with biosensors based on carbon nanotubes. TrAC Trends Anal Chem 45:24–36
65. Tang J et al (2013) Carbon nanodots featuring efficient FRET for real-time monitoring of drug delivery and two-photon imaging. Adv Mater 25(45):6569–6574
66. Liu H et al (2019) Lysosome-targeted carbon dots for ratiometric imaging of formaldehyde in living cells. Nanoscale 11(17):8458–8463
67. Mohammadinejad A et al (2023) Application of green-synthesized carbon dots for imaging of cancerous cell lines and detection of anthraquinone drugs using silica-coated CdTe quantum dots-based ratiometric fluorescence sensor. Spectrochim Acta Part A Mol Biomol Spectrosc 288:122200
68. Li H et al (2010) Water-soluble fluorescent carbon quantum dots and photocatalyst design. Angew Chem Int Ed 49(26):4430–4434
69. Xu L-D et al (2019) Ultrasensitive detection of severe fever with thrombocytopenia syndrome virus based on immunofluorescent carbon dots/SiO2 nanosphere-based lateral flow assay. ACS Omega 4(25):21431–21438
70. Mohammadinejad A et al (2017) Tandem determination of mitoxantrone and ribonucleic acid using mercaptosuccinic acid-capped CdTe quantum dots. J Lumin 190:254–260
71. Berlina AN et al (2013) Quantum-dot-based immunochromatographic assay for total IgE in human serum. Plos One 8(10):e77485
72. Li X et al (2012) A fast and sensitive immunoassay of avian influenza virus based on label-free quantum dot probe and lateral flow test strip. Talanta 100:1–6
73. Sheng W et al (2017) Visual and rapid lateral flow immunochromatographic assay for enrofloxacin using dyed polymer microspheres and quantum dots. Microchim Acta 184:4313–4321
74. Sapountzi EA et al (2015) Lateral flow devices for nucleic acid analysis exploiting quantum dots as reporters. Anal Chim Acta 864:48–54
75. Beloglazova NV et al (2017) Fluorescently labelled multiplex lateral flow immunoassay based on cadmium-free quantum dots. Methods 116:141–148
76. Chen J et al (2018) A facile fluorescence lateral flow biosensor for glutathione detection based on quantum dots-MnO2 nanocomposites. Sens Actuators B Chem 260:770–777
77. Wang Y et al (2009) Study of superparamagnetic nanoparticles as labels in the quantitative lateral flow immunoassay. Mater Sci Eng C 29(3):714–718
78. Eveness J et al (2009) Evaluation of paramagnetic particles for use in a resonant coil magnetometer based magneto-immunoassay. Sens Actuators B Chem 139(2):538–542

79. Marquina C et al (2012) GMR sensors and magnetic nanoparticles for immunochromatographic assays. J Magn Magn Mater 324(21):3495–3498
80. Makiranta JJ, Lekkala JO (2006) Modeling and simulation of magnetic nanoparticle sensor. In: 2005 IEEE engineering in medicine and biology 27th annual conference 2006. IEEE
81. Lago-Cachón D et al (2017) High frequency lateral flow affinity assay using superparamagnetic nanoparticles. J Magn Magn Mater 423:436–440
82. Oh S et al (2011) Analytes kinetics in lateral flow membrane analyzed by cTnI monitoring using magnetic method. Sens Actuators B Chem 160(1):747–752
83. Yang B et al (2019) Advances in optical assays for detecting telomerase activity. Luminescence 34(2):136–152
84. Jiang D et al (2019) Nanozyme: new horizons for responsive biomedical applications. Chem Soc Rev 48(14):3683–3704
85. Calabria D et al (2021) Recent advancements in enzyme-based lateral flow immunoassays. Sensors 21(10):3358
86. Tang Y et al (2015) Upconversion particles coated with molecularly imprinted polymers as fluorescence probe for detection of clenbuterol. Biosens Bioelectron 71:44–50
87. Zhao P et al (2014) Upconversion fluorescent strip sensor for rapid determination of vibrio anguillarum. Nanoscale 6(7):3804–3809
88. Kokko L, Lövgren T, Soukka T (2007) Europium (III)-chelates embedded in nanoparticles are protected from interfering compounds present in assay media. Anal Chim Acta 585(1):17–23
89. Sharma B et al (2013) High-performance SERS substrates: advances and challenges. MRS Bull 38(8):615–624
90. Li X et al (2017) A SERS nano-tag-based fiber-optic strategy for in situ immunoassay in unprocessed whole blood. Biosens Bioelectron 92:517–522